Romanian Reports in Physics, Vol. 65, No. 1, P. 186–192, 2013

CONDENSED MATTER

LOW TEMPERATURE TEM INVESTIGATION OF ELECTRON BEAM INDUCED DECOMPOSITION OF NANOCRYSTALLINE HYDROZINCITE INTO ZnO

LEONA C. NISTOR, SERGIU V. NISTOR* and DANIELA GHICA

National Institute of Materials Physics, POB MG-7, Magurele, Ilfov, Romania
Corresponding author: Tel. +40 21 369 185; Fax: + 40 21 369 0177
E-mail address: snistor@infim.ro

Received May 22, 2012

Abstract. The fast decomposition of hydrozincite [$Zn_5(CO_3)_2(OH)_6$] into ZnO observed in the transmission electron microscope could be slowed down and investigated *in situ* by operating the microscope at very low electron beam current densities and cooling the specimen down to –160 ^oC. Thus, it was possible to observe and pursue the distinct structural steps of the disruption of the hydrozincite lattice due to the energetic emission of H_2O and CO_2 gases. The initially formed disordered ZnO phase was found to further crystalize resulting in a mesoporous structure of small ZnO nanocrystals.

Key words: $Zn_5(CO_3)_2(OH)_6$, ZnO, nanoparticles, amorphous, decomposition, TEM.

1. INTRODUCTION

The thermal decomposition of the hydrozincite or zinc carbonate basic, with formula $Zn_5(CO_3)_2(OH)_6$, further abbreviated as ZCB, into zinc oxide (ZnO) has been in the last few years of renewed interest as a possible route for producing nanosized ZnO with a high concentration of substitutional transition metal (TM) ions. Such a route is favored by what seems to be the easier doping of the precursor ZCB with such ions [1]. The resulting nanostructured ZnO doped with TM ions could lead to an improved diluted magnetic semiconductor for spintronic applications [2–5].

In a recent Electron Paramagnetic Resonance (EPR) study correlated with thermal analysis (TA), X-ray diffraction (XRD) and transmission electron microscopy (TEM) measurements [6], we found out that the thermal decomposition in air/vacuum of the nanocrystalline ZCB occurs mainly in a narrow range (< 10 ^oC) of temperatures, just below 255 / 225 ^oC, resulting in a strongly disordered nanosized ZnO, which further crystalizes into a nanocrystalline material.

The formation of the disordered ZnO was attributed to the strong emission of CO_2 and H_2O gases expected to take place during the ZCB decomposition. Our attempts to directly observe this process and to study the morphology and microstructure of the resulting products by TEM at room temperature were unsuccessful. The investigated nanocrystalline ZCB did instantly transform into ZnO, even for reduced electron beam currents employed during the observations.

In an effort to overcome this difficulty, we performed TEM investigations at low temperatures by using the liquid nitrogen cooling holder of the microscope, a procedure by which the electron beam induced modifications of certain specimens, called "beam sensitive", are slowed down [7]. By operating the microscope at low electron beam current densities, we could thus observe and investigate *in situ* the distinct structural steps of the ZCB → ZnO transformation.

2. EXPERIMENTAL

The structural investigations were performed on samples from a batch of commercial, nominally pure, anhydrous ZCB from Alfa Aesar (code A14590).

The XRD investigations were performed with a Bruker D8 Advance XRD diffractometer, in the $\theta - \theta$ geometry with a Cu anode. The Rietveld refinement of the experimental data was performed with the Topas software from Bruker. The 2θ range of 10^o to 140^o was swept for higher accuracy of the refined lattice parameters values.

For the TEM investigations was employed a conventional JEOL 200 CX TEM instrument equipped with a tungsten electron gun for low beam intensity operation. The specimens were prepared by crushing ZCB samples, dispersing the resulting powder in ethanol and dropping it on holey carbon grids. In all TEM experiments, the specimens were inserted in the cooling holder of the microscope and cooled with liquid nitrogen till stabilized at a temperature of $-160\ ^oC$.

3. RESULTS AND DISCUSSION

The recorded XRD pattern of the investigated hydrozincite shown in Fig. 1 corresponds to the $Zn_5(CO_3)_2(OH)_6$ compound. The results of its Rietveld analysis are presented in Table 1 together with reference data. Fig. 1 shows a very good fit of the experimental diffractogram with the simulated one obtained with the parameters given in Table 1. The increased intensity of the observed (021) peak in comparison with its simulation reflects a corresponding preferential orientation, which is related to the plate-like, needle-like morphology of the sample. This will be further shown in the TEM images. The textured morphology also led to larger errors in the calculation of the average crystallite size [8].

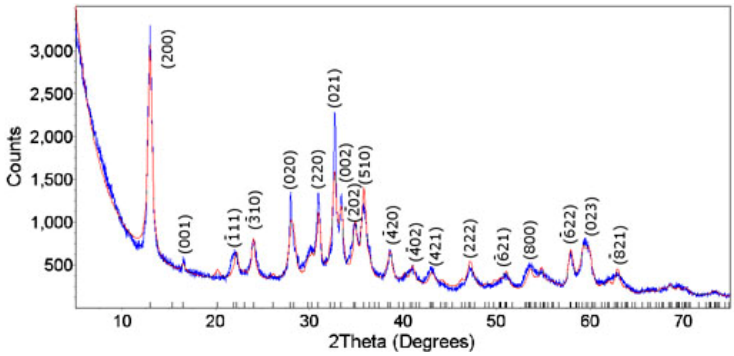

Fig. 1 – The XRD diffractogram of the ZCB and the superposed simulation with parameters from Table 1.

Table 1

The results of the Rietveld refinement of the XRD patterns from the presently investigated nanocrystalline ZCB batch in comparison with reference data

Sample	**Detected crystalline phase**	**Lattice parameters**	**Average crystallites size (nm)**
Anhydrous ZCB (Alfa Aesar code A14590)	$Zn_5(CO_3)_2(OH)_6$	$a = 13.70 \pm 0.04$ Å $b = 6.37 \pm 0.02$ Å $c = 5.38 \pm 0.02$ Å $\beta = 94.8^{o} \pm 0.5$	19
Reference sample ZCB [a]	$Zn_5(CO_3)_2(OH)_6$	$a = 13.58$ Å; $b = 6.28$ Å $c = 5.41$ Å; $\beta = 95.6^{o}$	–

[a] JCPD file no.19-1458.

Preliminary TEM investigations at room temperature revealed that, in a certain degree, the high sensitivity of the ZCB sample to the electron beam irradiation was also dependent on the size of ZCB nanocrystals which formed aggregates. According to the electron diffraction (ED) patterns, we found out that agglomerates of larger crystallites are more "stable" in the electron beam. Fig. 2 shows the time sequence of the ED patterns recorded at –160 ^{o}C, for the same aggregate of large ZCB crystallites, with the microscope operating at a beam current density much lower than in normal TEM illumination conditions. In this way, we were able to suitable lengthen the lapse of time in which the ZCB → ZnO transformation took place and, moreover, to reveal the distinct structural steps in which this transformation occurs. Fig. 2a presents the diffraction pattern recorded in the first 10 sec. of the measurement. It shows that the monoclinic $Zn_5(CO_3)_2(OH)_6$ structure has not yet been altered. The ED pattern contains spotty diffraction rings, corresponding to a polycrystalline specimen with rather large crystallites (up to a few 100 nm).

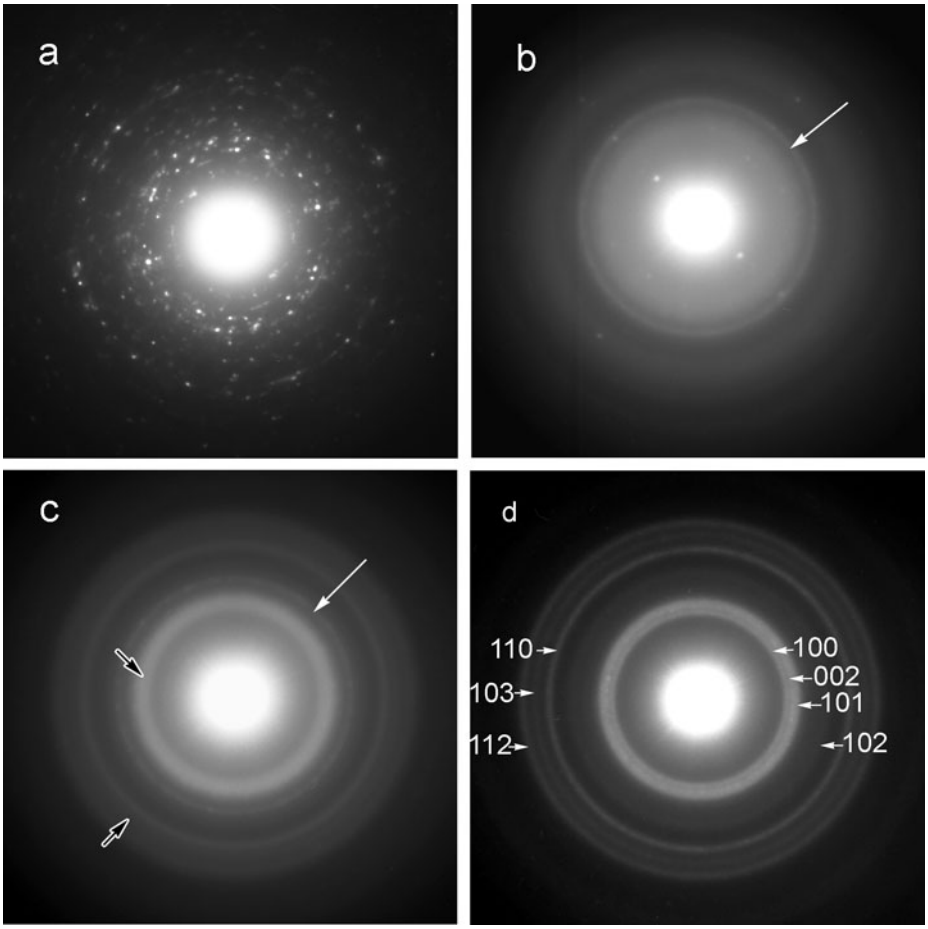

Fig. 2 – Sequence of ED patterns from the same agglomerate of the ZCB specimen exposed to a low current electron beam at –160 ^{o}C, for different lapses of time, showing the changes in specimen structure during the ZCB → ZnO transformation; white arrow indicates ZCB, black arrows indicate ZnO: a) 0 min, crystalline ZCB; b) 1 min, collapsed lattice of ZCB; c) 5 min, disordered ZnO and traces of ZCB; d) 10 min, indexed ED pattern of nanocrystalline ZnO.

After 1 min. of exposure to the low current electron beam, the ED pattern (Fig. 2b) shows the collapse and partial amorphization of the specimen structure, with few spots and a diffraction ring (marked with a white arrow) corresponding to hydrozincite. After subjecting the specimen for 5 min. to the electron beam, the recorded electron diffraction pattern (Fig. 2c) reveals the emergence of a disordered ZnO structure, while the residual ring (marked with a white arrow) from the ZCB structure is still present. The diffraction rings corresponding to ZnO are so wide that they overlap into two groups corresponding to the strongest diffraction maxima of the ZnO structure, marked by black arrows in Fig. 2c. About 10 min. of

exposure to the electron beam in the cooling holder was necessary to complete the transformation of the ZCB phase into a poorly crystallized ZnO phase (Fig. 2d). During the lapse of time of continuous electron irradiation which passed between the recordings of Fig. 2c and Fig. 2d, the crystallization of the newly formed disordered ZnO phase took place. Thus, the two groups of diffraction rings marked by black arrows in Fig. 2c tend to separate in Fig. 2d into distinct diffraction rings, resulting in the following determined values for the interplanar distances d_{hkl}: 0.28 nm, 0.26 nm and 0.25 nm for the diffraction rings of the first group and 0.16 nm, 0.15 nm and 0.14 nm for the diffraction rings of the second group, respectively. Since the measured d_{hkl} values are very close to those given in the JCPD file 89-137 for the wurtzite structure of ZnO, the diffraction pattern of Fig. 2d could be correspondingly indexed. It is worth mentioning that the diffraction pattern of Fig. 2d still exhibits rather wide diffraction rings, corresponding to very small ZnO nanocrystallites (< 5 nm).

Fig. 3 presents the sequence of TEM images of the same aggregate of crystallites on which the sequence of diffraction patterns of Fig. 2 were recorded. Each TEM image was recorded at a low electron beam current, subsequent to the recording of its corresponding electron diffraction pattern. The TEM images reveal changes in the specimen morphology while subjected to the electron beam in the cooling holder. Fig. 3a presents the characteristic morphology of the ZCB sample consisting of agglomerates of thin plate-like and needle-like crystallites.

After a longer exposure to the low current electron beam, clear changes in the morphology of the investigated ZCB sample were observed. Although the general plate- and needle-like morphology was still recognizable, the collapse of the structure, as revealed in the electron diffraction pattern from Fig. 2b, is also evident in the TEM image of the Fig. 3b. The image is fuzzy, the ZCB plates or needles are crumbled into smaller crystallites (some of 5–6 nm). Pores are formed, accompanied by a slight shrinking of the whole agglomerate, better visible in Fig. 3c which shows the emerging disordered ZnO compound. The morphology modifications are the direct result of a strong mass loss by the intense release of CO_2 and H_2O gases in the vacuum of the microscope column. This process takes an "eruptive" character, observed as a boiling like movement of the sample, also reflected in the blurring of the images taken before the ZCB → ZnO transformation is complete (Figs. 3a and 3b).

Fig. 3d presents the TEM image of the completely transformed specimen at higher magnification, representing to the central part of the previous images. Its corresponding electron diffraction pattern is given in Fig. 2d. It reveals the morphology of the mesoporous, nanocrystalline ZnO phase, which emerged from the decomposition of ZCB phase. The dimensions of the resulted ZnO nanoparticles initially formed in the ZCB → ZnO transformation are in the 1.5 to 2.5 nm range.

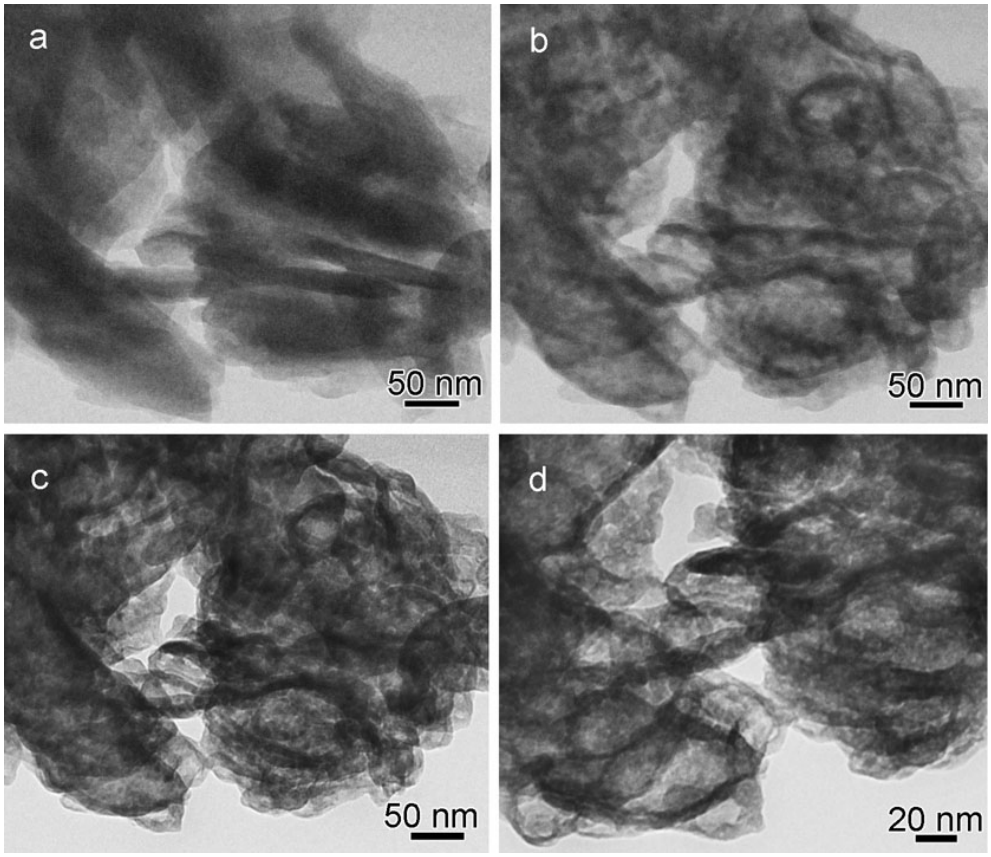

Fig. 3 – Sequence of TEM images corresponding to the ED patterns of Fig. 2, from the same agglomerate of the ZCB specimen exposed to a low current electron beam at –160 ^{o}C, for different lapses of time: a) 0 min; b) 1 min; c) 5 min; d) 10 min, showing the changes in specimen morphology during the ZCB → ZnO transformation.

4. CONCLUSIONS

We have been able to observe by TEM, on an extended time scale of several minutes, the structural changes related to the decomposition in the electron beam of the nanocrystalline ZCB into ZnO, which in normal, room temperature operation conditions takes place instantly. This has been possible by cooling the sample down to -160 ^{o}C and employing a very low electron beam current density during the observations. In these conditions, the transformation of the ~ 100 nm size ZCB nanocrystals into a disordered, quasi-amorphous ZnO phase took place in about 5 minutes, as revealed by the electron diffraction patterns (Figs. 2a–2c). During this time an energetic, eruptive-like degassing process, due to the release of H_2O and CO_2 gases has been observed, which explains the crumbling of the ZCB lattice in

very small, disordered nanoparticles and the formation of pores. Further observations both in electron diffraction and imaging modes evidenced a slow crystallization process with the formation of ZnO nanocrystals of much smaller size compared to the initial ZCB nanocrystals.

The present study confirms the results of a previous EPR investigation [6] concerning the thermal decomposition of the nanocrystalline ZCB phase into a strongly disordered, quasi-amorphous ZnO phase, which further crystalizes into small sized nanocrystalline material. It also demonstrates that the initial formation of the disordered ZnO phase is due an energetic, eruptive-like degassing process which breaks down the ZCB nanocrystallites into much smaller ZnO nanoparticles.

Acknowledgements. This work was supported by CNCSIS-UEFISCSU, project number PN-II-IDEI-523/2008.

REFERENCES

1. Z. Mickovic, D. T. L. Alexander, A. Sienkiewicz, M. Mionic, L. Foro and A. Magrez, Cryst. Growth & Design, **10**, 4437 (2010).
2. T. Dietl, H. Ohno, F. Matsukura, J. Ciebert and D. Ferrand, Science, **287**, 1019 (2000).
3. K. Sato and H. Katayama-Yoshida Phys. Stat. Sol., **B 229**, 673 (2002).
4. J. M. D. Coey, M. Venkatasan and C. B. Fitzgerald, Nature Mater. **4**, 173 (2005).
5. N. S. Norberg, K. R. Kittilstved, J. E. Amonete, R. K. Kukkadapu, D. A. Schwartz and D. R. Gamelin, J. Am. Chem. Soc., **126**, 9387 (2004).
6. S. V. Nistor, L. C. Nistor, M. Stefan, D. Ghica, Gh. Aldica and N. J. Barascu, Cryst. Growth & Design, **11**, 5030 (2011).
7. L. W. Hobbs, *Introduction to Analytical Electron Microscopy*, J. J. Hren, J. I. Goldstein and D. C. Joy (Editors), Plenum Press, New York, 1979.
8. C. Weidenthaler, Nanoscale, **3**, 792 (2011).